Vol. 32 (2001) *ACTA PHYSICA POLONICA B* No 2

CONDUCTIVITY AND THERMOPOWER IN ROPES OF CARBON NANOTUBES — A TIGHT BINDING MODEL APPROACH*

T. Kostyrko[a] and M. Bartkowiak[a,b,c]

[a]Institute of Physics, A. Mickiewicz University
Umultowska 85, 61-614 Poznań, Poland
[b]Department of Physics and Astronomy, University of Tennessee
Knoxville, TN 37996-1200, USA
[c]Solid State Division, Oak Ridge National Laboratory
Oak Ridge TN 37831-6030, USA

(Received October 30, 2000)

We analyze the doping dependence of the thermopower and conductivity of ropes of single wall carbon nanotubes using a tight binding model. A sizeable value of the Seebeck coefficient in these systems together with its Fermi liquid like temperature behavior indicate an asymmetry near the Fermi surface. We discuss two possible explanations for this asymmetry of the electronic structure of the nanotube ropes, one due to defect states, another resulting from the intertube interactions.

PACS numbers: 73.20.Dx, 72.80.Rj, 85.30.Vw

1. Introduction

The transport properties of the ropes of single wall carbon nanotubes (NTs) [1] exhibit several so far unexplained features:

1. Substantial value of the thermopower (TEP) which increases initially linearly with temperature like in the Fermi liquid [2–4]. This is surprising because the band structure calculations performed for the individual NT does not show much [5] (or any [6]) asymmetry around the Fermi surface and TEP should vanish in such a case.

---

[*] Presented at the XXIV International School of Theoretical Physics "Transport Phenomena from Quantum to Classical Regimes", Ustroń, Poland, September 25–October 1, 2000.

2. The electrical conductivity measured on undoped mats of ropes of NTs first slowly increases with decrease of temperature then, upon reaching some temperature minimum, starts to decrease rapidly. This low temperature decrease may be understood as onset of a weak localization [7, 8] and is not unlike to the behavior observed in the doped polyacetylene, where it was described using a variable range hopping model [9].

3. Upon doping with either hole or electron donors conductivity can be considerably enhanced (even up to 120 times for Cs-doped NT mats [10]). At the same time, the K-doped mats no longer show the resistivity increase in low temperature region [11].

4. The conductance measurements made on the individual rope on NTs show irregular fluctuations with the gate voltage, which may be due to the defect states. The doping of the single rope *in situ* with K atoms, increases the conductance by a factor of 20 at $T = 5.3$ K [11], and at the same time the fluctuations disappear. This fact is in contradiction with expectations of increased role of disorder due to introduced dopant ions.

5. The transport properties of NTs were shown to be very sensitive to the presence of oxygen in their environment [12, 13]. The gas acts probably as the electron acceptor, shifting the position of the Fermi level downwards by a fraction of eV. This in agreement with observation of a chemical potential shift in multiwall carbon nanotubes [14] as well as the known charge transfer from the oxygen to planar defected graphite [12]. The surprisingly large TEP of *degassed* NTs indicates, however, an "important asymmetry in the electronic carbon π bands" near the Fermi energy [13].

In this paper we try to understand qualitatively the general features of the transport properties of the NT ropes, with a help of simple calculations using a tight binding model of these systems. At present the nature of scattering processes which determine the temperature behavior of the conductivity and the thermopower is not clear. Here we assume that the electron scattering is due mainly to the presence of defects.

In Section 2 we consider influence of the doping on transport properties of an individual NT. We restrict our attention to armchair NTs, which are gapless and therefore exhibit metal-like properties. We calculate the position of the Fermi level of the NT as a function of electron concentration. We estimate the resistance of the NT in a semiclassical approximation, neglecting interference in scattering from different defects. This will allow us to derive an approximate result for the thermopower as a function of electron or hole doping for a wide range of doping.

In the Section 3 we analyze the influence of the intertube interactions on the asymmetry of the electronic structure near the Fermi level (for undoped tubes). We calculate the influence of this asymmetry on the conductivity and the thermopower in the rope of NT for small electron and hole doping.

In Section 4 we discuss the above mentioned experimental facts in the light of our computations.

2. Transport properties of an individual NT

2.1. Doping dependence of the Fermi level in an individual NT

A Hamiltonian of the system of noninteracting armchair NTs can be written as

$$\mathcal{H}_0 = \sum_{\rho j} \left[\Psi^\dagger_{\rho j} \begin{pmatrix} H_a & W \\ W & H_b \end{pmatrix} \Psi_{\rho j} + \left(\Psi^\dagger_{\rho j} \begin{pmatrix} 0 & 0 \\ t & 0 \end{pmatrix} \Psi_{\rho j+1} + \text{h.c.} \right) \right] . \qquad (1)$$

In above, Ψ represents a $4N_a$-dimensional vector of electron operators of (N_a, N_a) armchair NT for the j cell of the NT in a position defined by a vector ρ, $\Psi^\dagger_{\rho j} = (a^\dagger_{\rho j}, b^\dagger_{\rho j})$. The $2N_a \times 2N_a$ dimensional matrices H_a, H_b describe hopping processes within subsystems of a and b orbitals. W describes hopping between a and b type orbitals within the same cell. t is an intercell hopping matrix between a and b orbitals. The specific forms of these matrices are defined in [16]. The hopping parameter between NN carbon atoms is here $t = -3$ eV. Writing the Hamiltonian of the NT in the form of Eq. (1) we assume that effects of Coulomb interactions may be treated within a one-particle approach and the hopping integrals include the effect of interaction by means of Hartree–Fock approximation. The effect of the interactions on the site energy (*i.e.* Hartree term) leads in the case of individual NT to a uniform shift of all bands because all sites are equivalent (we do not consider a possibility of the CDW state here).

In this work we assume periodic boundary condition in direction parallel to the NTs axis (which is justified for long enough NTs). In this case energy spectrum of an individual NT can be explicitly obtained [1]

$$\varepsilon_{k\nu s} = s\, t \sqrt{1 + 4\cos\frac{k}{2}\, \cos(q_\nu) + 4\cos^2\frac{k}{2}}\,, \quad s = \pm 1 \qquad (2)$$

where $q_\nu = \pi\, \frac{\nu}{N_a}$, $\nu = 1 \ldots 2N_a$, $\nu \neq N_a$ and $|k| < \pi$ [15]. For $\nu = N_a$ one has

$$\varepsilon_{k\, N_a s} = s\, t \left(1 - 2\cos\frac{k}{2} \right) . \qquad (3)$$

For undoped NT, only two bands with $\nu = N_a$ and $s = \pm 1$ cross the Fermi surface, which takes place for $k = \pm\frac{2\pi}{3}$. The band structure for (10,10) NT is shown in Fig. 1. We have $4N_a$ bands for (N_a, N_a) NT, corresponding to $4N_a$ atoms in the unit cell of the armchair NT $1-d$ lattice, some of them are degenerate. The bands for which $\alpha_\nu = \cos(q_\nu) > 0$ $(\nu = \frac{N_a}{2}, \ldots, 2N_a)$, are monotonous functions of the wave vector and may cross the Fermi level at two points. The bands with $\alpha_\nu < 0$, which have minimum at some point k_0, $(0 < k_0 < \pi)$ may cross the Fermi level in two or four points. One has for $\alpha_\nu < 0$ (below I drop s index and consider only $s = +1$ bands, except the one with $\nu = N_a$)

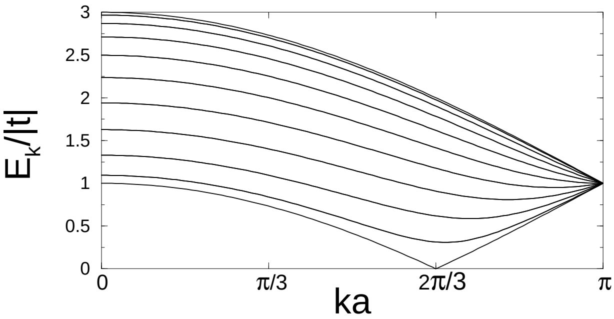

Fig. 1. Band structure of (10,10) NT.

$$\rho_\nu(\omega) = \frac{1}{\pi}\int\limits_{\varepsilon_{k_0\nu}}^{\varepsilon_{\nu 0}} \frac{d\varepsilon}{|v_\nu^{(-)}(\varepsilon)|}\delta(\omega-\varepsilon) + \frac{1}{\pi}\int\limits_{\varepsilon_{\nu k_0}}^{\varepsilon_{\nu\pi}} \frac{d\varepsilon}{|v_\nu^{(+)}(\varepsilon)|}\delta(\omega-\varepsilon)\,, v_{\nu k} = \frac{d\varepsilon_{\nu k}}{dk}\,, \quad (4)$$

where the velocity $v_{\nu k}$ is represented as a function of the energy for the given band, by inverting Eq. (2). The result is

$$\begin{aligned}
&\rho_\nu(\omega) = \rho_\nu^{(-)}(\omega) + \rho_\nu^{(+)}(\omega)\\
&= \frac{\theta(\omega-\varepsilon_{\nu k_0})\theta(\varepsilon_{\nu 0}-\omega)}{\pi|v_\nu^{(-)}(\omega)|} + \frac{\theta(\omega-\varepsilon_{\nu k_0})\theta(\varepsilon_{\nu\pi}-\omega)}{\pi|v_\nu^{(+)}(\omega)|}\\
&= \frac{\omega/|t|t}{\pi\sqrt{\alpha_\nu^2+\omega^2/t^2-1}}\left[\frac{\theta(\omega - t\sqrt{1-\alpha_\nu^2})\theta(t-\omega)}{\sqrt{1-\alpha_\nu^2+(1-\omega^2/t^2)/4-\frac{\alpha_\nu}{2}\sqrt{\alpha_\nu^2+\omega^2/t^2-1}}}\right.\\
&\left.+\frac{\theta(\omega-t\sqrt{1-\alpha_\nu^2})\theta(t\sqrt{5+4\alpha_\nu}-\omega)}{\sqrt{1-\alpha_\nu^2+(1-\omega^2/t^2)/4+\frac{\alpha_\nu}{2}\sqrt{\alpha_\nu^2+\omega^2/t^2-1}}}\right] \qquad (5)
\end{aligned}$$

for $\alpha_\nu < 0$ and for $s = +1$. For $\alpha_\nu > 0$, $s = +1$ one has

$$\begin{aligned}\rho_\nu(\omega) &= \frac{\theta(\omega - \varepsilon_{\nu 0})\theta(\omega - \varepsilon_{\nu\pi})}{\pi|v_\nu^{(+)}(\omega)|} \\ &= \frac{\omega/|t|t}{\pi\sqrt{\alpha_\nu^2 + \omega^2/t^2 - 1}} \frac{\theta(\omega - t\sqrt{1-\alpha_\nu^2})\theta(t\sqrt{5+4\alpha_\nu} - \omega)}{\sqrt{1 - \alpha_\nu^2 + (1-\omega^2/t^2)/4 + \frac{\alpha_\nu}{2}\sqrt{\alpha_\nu^2 + \omega^2/t^2 - 1}}} \, . \end{aligned} \tag{6}$$

For $\nu = N_a, s = +1$ one gets

$$\rho_{N_a}(\omega) = \frac{\theta(t^2 - \omega^2)/|t|}{\pi\sqrt{1 - (1-\omega/t)^2/4}} \, . \tag{7}$$

The DOS for subbands with $s = -1$ may be obtained from the relation: $\rho_{\nu,s}(\omega) = \rho_{\nu,-s}(-\omega)$. In Fig. 2 we show the total density of states (normalized to 1) of the (10,10) NT for $\omega/t > 0$,

$$\rho(\omega) = \frac{1}{4N_a} \sum_{\nu s} \rho_{\nu s}(\omega) \, .$$

The $1 - d$ van Hove singularities seen at $\omega = t\sqrt{1 - \alpha_\nu^2}$, $t\sqrt{5 + 4\alpha_\nu}$ correspond to band minima and maxima, respectively (see Fig. 1).

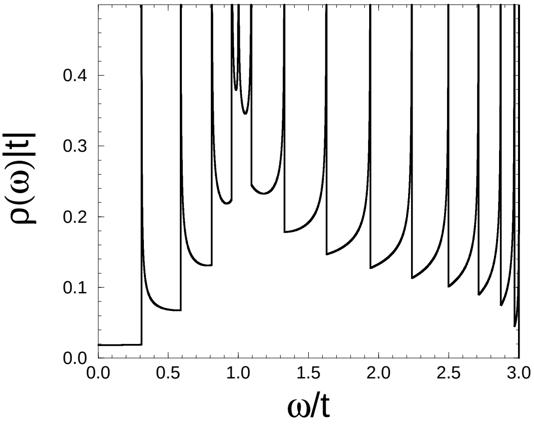

Fig. 2. Density of states of (10,10) NT.

At half filling (undoped NT) the Fermi energy is positioned at $\omega = 0$. Doping with K will shift the position of the Fermi level in such a way that for the limiting (unrealistic) case CK$_1$ the band system will be completely full. In Fig. 3 we show the position of the Fermi level as a function of, say,

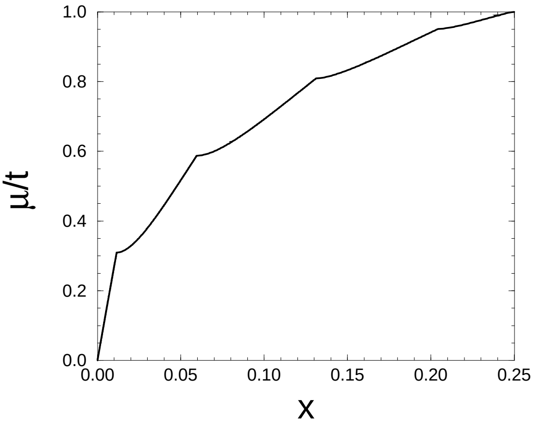

Fig. 3. Dependence of the position of the Fermi level on K doping in (10,10) NT for $x < 0.25$.

K-doping for the NT compound CK_x. (The picture is the same for electron and hole doping because the band structure is completely symmetric here).

One can note that very small doping ($x \approx 0.0115$ for (10,10) NT) is sufficient to shift the Fermi level to the position of the first van Hove singularity in DOS which is at $\omega/t = \sin[\pi/N_a]$ =($\approx \pm\pi/N_a$ for $N_a \approx 10$). Note that Fermi energy increases initially linearly with x. More precisely, by integration of DOS one obtains, for $|\mu/t| < \sin(\pi/N_a)$

$$x = \frac{1}{\pi N_a}\left[\arcsin\left(\frac{1+\frac{\mu}{t}}{2}\right) - \arcsin\left(\frac{1-\frac{\mu}{t}}{2}\right)\right], \tag{8}$$

$$\frac{\mu}{t} = \frac{\sqrt{3}\pi N_a}{2}x + \ldots . \tag{9}$$

The linear term in x of Eq. (9) gives about 1% accuracy, until μ reaches first van Hove singularity.

2.2. Resistance of the NT in the semiclassical approximation

According to the Landauer theory [17] the conductance of a mesoscopic sample in $T \to 0$ limit may be related to a reflection coefficient R with a formula

$$\Gamma = \Gamma_0\,(1-R), \quad \text{where} \quad \Gamma_0 = \frac{e^2 n_c}{h}\,. \tag{10}$$

Here n_c denotes the number of conducting channels. The coefficient R measures a probability of an electron reflection from the sample and its return to the lead from which it was injected. R is measured at the Fermi level. The limit of the maximum conductance, Γ_0, is obtained for the vanishing reflection, in the case when the only source of scattering is the contact between the sample and the measuring leads. For macroscopic samples the main factor limiting the conductance is usually the scattering of the electrons within the sample, by defects or interactions of electrons with other quasiparticles. It is convenient to separate the contact contribution to the total resistance, $\mathcal{R}_{\rm c} = 1/\Gamma_0$ from the total resistance, $\mathcal{R} = 1/\Gamma$ and rewrite $\mathcal{R}$ in the form

$$\mathcal{R} = \mathcal{R}_{\rm c} + \mathcal{R}_{\rm i}, \quad \mathcal{R}_{\rm i} = \mathcal{R}_{\rm c}\frac{R}{1-R}\,. \tag{11}$$

Above $\mathcal{R}_{\rm i}$ denotes the internal ('actual' [17]) resistance related to the properties of the sample itself. $\mathcal{R}_{\rm i}$, which may be measured directly in the four lead measurement, is determined by the potential drop within the sample and may vanish in absence of defects. The internal resistance may be readily obtained in the case of a single point-like defects, by calculation of the reflection R from the scattering theory. The exact computation for a large number of the defects is difficult due to effects of interference between electron waves scattered from the different defects. The interference effects, which manifest as very irregular fluctuations of the conductance of the sample, lead eventually to localization of electron states and vanishing of the conductance (at $T = 0$) in the limit of an infinitely long sample. For a not too long sample or a small enough number of the defects, in between the ballistic limit and the localized one, we may neglect the interference effects and still obtain fair enough qualitative description of the resistance. The neglect of the interference effects may also be justified in the presence of other scattering processes (due to phonons, unpaired spins, electron–electron interactions, intertube hopping), which break the phase coherence of the carriers between the consecutive elastic collisions with defects within the NT. The reflection of a sample containing m identical defects, obtained in the approximation neglecting the interference effects, reads [18]

$$R_m = \frac{m\,R_1}{1+(m-1)\,R_1}\,, \tag{12}$$

where R_1 denotes a reflection of the sample with a single defect. Using Eqs. (11),(12) we obtain the approximate expression for the internal resistance, which obeys the Ohm's law [17]

$$R_{\Omega}(m) = R_{\rm c}\,m\,\frac{R_1}{1-R_1}\,. \tag{13}$$

In Fig. 4 we show the internal conductance per single defect, $\sigma{=}m/R_{\Omega}(m)$, as a function of the Fermi level μ. We used here the values of the single point defect reflection R_1 obtained with a help of the transfer matrix method [16]. We show here the results obtained for *positive* values of $E_{\rm d}$, which correspond to electron donor substitution. The results for negative values of $E_{\rm d}$ may be deduced from the presented figures by a replacement: $\mu \to -\mu$. The calculation for the weak defects ($E_{\rm d}/|t| = 0.1$) are similar to what one obtains from the Boltzmann theory applied to the $1-d$ system, with the relaxation time calculated using the Born (*i.e.* second order with respect to $E_{\rm d}$) approximation,

$$\sigma_{\rm B}(\mu) = \frac{e^2}{\pi^2}\sum_{\nu}\frac{\tau(\mu)}{\rho_\nu(\mu)}, \qquad \tau^{-1}(\mu) = \frac{1}{\hbar}\sum_{\nu}\rho_\nu(\mu)E_{\rm d}^2\,. \tag{14}$$

The equivalence of the two approaches may be explicitly shown in $E_{\rm d} \to 0$ limit using the results for the single defect reflection R_1 [18,19]. However, even in the case of the weak defect $E_{\rm d}/|t| = 0.1$ one can see clearly the quantitative differences of these results. The scattering time from the Born approximation [20] leads to the result for σ which is symmetric with respect to $\mu = 0$ and is only weakly dependent on μ in the central two band region, $-\pi/10 < \mu/|t| < \pi/10$. On the contrary, the expression for R_1 includes single defect scattering exactly and leads to a noticeable asymmetry in σ. The asymmetry increases with increase of the defect strength. For the very large value of $E_{\rm d}$ the reflection R_1 exhibits the maximum corresponding to appearance of the quasibound state within the two band region [16] and at this point the internal conductance is strongly suppressed.

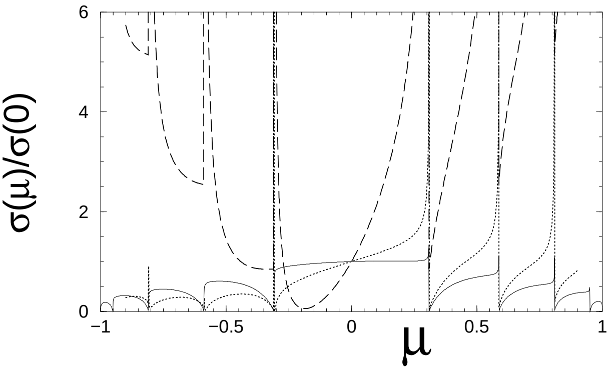

Fig. 4. Internal conductance per single defect for the (10,10) nanotube as a function of the Fermi level (in units of $|t|$) at $T = 0$ K. Thin line: $E_{\rm d}/|t| = 0.1$, dotted line: $E_{\rm d}/|t| = 1$, dashed line: $E_{\rm d}/|t| = 6$.

In the real system one may expect the internal resistance which is approximately the weighted average of the contributions from different defects. In particular, the amount of the oxygen adsorbed at the NT walls may be probably estimated from the shift of the chemical potential with respect to $\mu = 0$, *i.e.* it is the order of 1% or less. If it exist in a form of the negatively charged ion, it may probably raise the site energy of the neighboring carbon atoms by a value of order of several eV. The topological Stone–Wales, or 5–77–5, defect may be approximately represented (for $\omega = 0$) by the strong point defect, $E_{\rm d}/|t| \sim 6$ [16], and it was estimated to appear once in every 10^5 C–C bonds [21]. Unfortunately, little is known about frequency of appearance of other defects (NT bending, vacancies, 5–7 pairs...), what precludes systematic quantitative comparison with experiments. One may wonder, however, if the present results allow to understand the doping dependence of the conductance, mentioned in the Introduction. The saturation intake of the potassium is probably close to $x = 0.125$, which corresponds the chemical potential shift $\Delta\mu/|t| \sim 0.8$, with respect to $\mu = 0$. Assumption, that the only effect of doping is the chemical potential shift, does not explain the increase of the conductance in the case of the dominating weak defect (see Fig. 4, thin solid line for $E_{\rm d}/|t| = 0.1$) because in this case the conductance *decreases* by a factor of 2. This may be understood in part as the effect of the relatively low Fermi velocity at the shifted Fermi level (see Fig. 1). Indeed the number of the conducting bands increases 5-fold, but the average Fermi velocity decreases to about 75% of its value at $\mu = 0$. The more important effect comes from the enhanced scattering due to the increased, by a factor of 6, density of states at $\mu/|t| \sim 0.8$ as compared to $\rho(\mu = 0)$ (see Fig. 2). The resulting decrease of conductance to about $5 \times 0.75/6 = 0.625$ of its value at $\mu = 0$ is seen in Fig. 4.

The situation is similar in the case of the moderate ($E_{\rm d}/|t| = 1$) defect. Only the dominance of the strong defects changes the situation radically and the conductance may considerably increase as the Fermi level moves far from the vicinity of the quasibound state (see Fig. 4 for $E_{\rm d}/|t| = 6$). Also the factors not included in the model may be responsible for the increase of the conductance for the strong doping. One of the most important ones is the increase of the number of conducting NTs in the rope from the original fraction of $\frac{1}{3}$ to unity. Another possible effect is a better screening of the charged defects (including the dopant ions) due to increased density of charge carriers. Indeed, the measurement of the gate voltage dependence of the pristine and K-doped rope shows an almost featureless and voltage independent conductance in the doped rope as compared to strongly oscillating and asymmetric with respect to $V_{\rm G} = 0$ dependence in the undoped rope. At the same time the low temperature upturn of the resistance with $T \to 0$ K is either reduced (in the single rope) or completely suppressed (in NTs mats) for the doped samples. These facts suggest the decrease of the effective value of the defect strength as a result of the doping.

2.3. Thermoelectric power

The standard approach to the low temperature thermopower uses the Mott formula

$$S = \frac{\pi^2 k_{\mathrm{B}}^2 T}{3e} \frac{d \log \sigma(\mu)}{d\mu}\,. \tag{15}$$

The linear contribution to S, indicated by Eq. (15), has been indeed observed [3], although the general temperature behavior of the NT mats is more complicated. The variation and the substantial value of the thermopower was interpreted as resulting from the unpaired spins of transition metal ions [3] (Kondo effect) or due to presence of semiconducting NTs in the ropes [2]. Here we consider a contribution coming from a substantial energy variation of the conductance, which may be related to local defects and the vicinity of the quasibound state minimum in the conductance.

We restrict our discussion to small enough doping that the Fermi level stays within the central two band system, $-\pi/10 < \mu/|t| < \pi/10$, *i.e.* $x < 0.01$. We assume that the conductivity of the whole system is proportional to the conductance of the single rope. In this case we can use the result for σ obtained above to determine the thermopower with a help Eq. (15). We assume for simplicity that only one kind of defect is present in the system. Generalization to several types of defects is easy, in this case S would depend on the defects concentration and would vary between the value calculated for strong and weak defects taken separately.

In Fig. 5 we show the value of $d\log[\sigma(\mu)]/d\mu$ corresponding to the computed resistance presented in Fig. 4. To obtain the thermopower from the results showed in Fig. 5 we have to multiply the derivative by the prefactor $(\pi^2/3)(k_{\mathrm{B}}/e)(k_{\mathrm{B}}T/|t|)$ from Eq. (15) which is equal to $\approx 8\times10^{-3}\,T$ [μV/K], where T is given in Kelvin degrees. For example, the value of TEP corre-

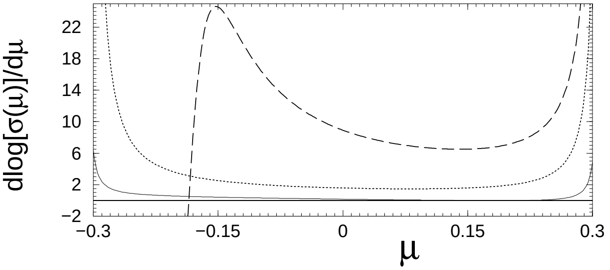

Fig. 5. The derivative of the logarithm of conductance with respect to the position of the Fermi level, for the (10,10) nanotube as a function of the Fermi level (in units of t) at $T = 0$ K. Thin line: $E_{\mathrm{d}}/|t| = 0.1$, dotted line: $E_{\mathrm{d}}/|t| = 1$, dashed line: $E_{\mathrm{d}}/|t| = 6$.

sponding to $d\log(\sigma)/d\mu = 2$ in Fig. 5 and extrapolated to $T = 300$ K, is equal to $8 \times 10^{-3} \times 3 \times 10^{2} \times 2 \approx 5$ [μV/K].

As follows from the presented results, the absolute value of the thermopower depends considerably on the defect strength. For the weak–to–moderate value of $E_{\rm d}$ ($E_{\rm d}/|t| < 1$) the derivative of $\log(\sigma)$ changes rather weakly with μ. The exception is the behavior of the derivative close to the van Hove singularities at $\pm\sin(\pi/10)$ where, however, application of Eq. (15) is questionable. The calculated figures correspond to TEP of order of few μV/K at $T = 300$ K. Note, that the positive value of $d\log(\sigma)/d\mu$ corresponds to electron–like charge carriers, and would change sign with the sign change of $E_{\rm d}$.

The situation is very much different for the strong defect, which leads to the formation of the quasibound state. The derivative of $\log(\sigma)$ may reach quite substantial values, corresponding (for $E_{\rm d}/|t| = 6$) to TEP not less than $\sim 20\mu$V/K at $T = 300$ K. At the position of the quasibound state minimum in σ the derivative changes sign. On the left side of the minimum the thermopower is hole–like, on the right electronlike. Note that the change of sign of $E_{\rm d}$ does not change the last conclusion — for the negative value of $E_{\rm d}/|t|$ the corresponding zero of TEP will only be shifted to a positive value of μ. In the limiting case $E_{\rm d}/|t| \to \infty$ (which is sometimes used to mimic a carbon vacancy), σ is symmetric with respect to change $\mu \to -\mu$ and the change of sign of $E_{\rm d}$ does not change the value of $d\log(\sigma)/d\mu$ at all.

3. Transport properties of ropes of NTs

3.1. Tight binding model for a rope of NTs

We form a model of crystalline rope of the NTs by all possible translations of a copy of the individual NT by all vectors of the triangular Bravais lattice, perpendicular to the NT's z-axis. The resulting (infinite) lattice is perfectly periodic although it does not in general possess the inversion symmetry. The exceptions are the cases of $N_a = 6, 12, 18\ldots$ for arrangements with NT's symmetry axis coinciding with symmetry axis of the triangular lattice. Intertube hopping processes in thus obtained lattice can be described by a Hamiltonian [22]

$$\mathcal{H}_1 = \sum_{s=0,\pm1;\rho\varDelta} \left(\varPsi^{\dagger}_{\rho j} \mathcal{T}_{\varDelta s} \varPsi_{\rho+\varDelta j+s} + \text{h.c.} \right) , \tag{16}$$

$$\text{where:} \quad \mathcal{T}_{\varDelta s}, = \begin{pmatrix} V^{a}(\varDelta s) & V^{ab}(\varDelta s) \\ V^{ba}(\varDelta s) & V^{b}(\varDelta s) \end{pmatrix} .$$

Here $\varDelta$ is a vector joining nearest neighbors of the triangular lattice. The $4N_a \times 4N_a$ matrix $\mathcal{T}_{\varDelta s}$ describes all hopping processes between orbitals of the j-cell of NT in position ρ and m-cell of NT in position $\rho + \varDelta$. In above we restricted ourselves to the hopping processes between j and m cells of neighboring NTs to the ones with $j = m$ and $j = m \pm 0, 1$.

Besides appearance of the intertube hopping the electron states of the individual NTs can be modified as a result of Coulomb interaction between electrons from the different nanotubes. Now however, because the carbon sites are no longer equivalent, the corresponding Hartree terms may lead to a site dependent potential with symmetry of the triangular lattice. This additional local potential may be accounted for by change of the diagonal elements of matrices H_a, H_b in Eq. (1).

We can use the periodicity of the total Hamiltonian, and rewrite it using space Fourier transform of the site operators $\varPsi_{\rho j}$,

$$\varPsi_{\rho j} = \frac{1}{N_\perp N_{||}} \sum_{kq} \mathrm{e}^{ikj + iq\rho} \varPsi_{kq} \,,$$

where $N_\perp, N_{||}$ represent the number of NTs in the bundle and the number of the cells in each NT. The Hamiltonian can be now rewritten as

$$\mathcal{H} = \sum_{kq} \left[\varPsi_{kq}^\dagger \begin{pmatrix} H_a + \delta_a & W + t^\dagger \exp(-ik) \\ W + t \exp(ik) & H_b + \delta_b \end{pmatrix} \varPsi_{kq} + \varPsi_{kq}^\dagger \mathcal{T}_{kq} \varPsi_{kq} \right] , \tag{17}$$

where δ_a, δ_b represent change of the site energy due to assembling of the NT to form a rope and the Hermitian matrix $\mathcal{T}_{kq}$ is a Fourier transform of the intertube hopping one. The Hamiltonian in Eq. (17) can be diagonalized easily with a help of canonical transformation. However, such a procedure involves diagonalization of $4N_a \times 4N_a$ matrices with rather irregular distribution of elements and one can hardly hope to get explicit result. Instead we work in the representation in which the part $\mathcal{H}_0$ of Eq. (17) is made diagonal with a help of a transformation, $\varPsi_{kq} = f_k \varPhi_{kq}$ (the detailed form of the unitary matrix f_k is given in [16]). The intertube Hamiltonian can be then treated analytically as a perturbation.

In the new representation the intertube part of the Hamiltonian takes a form

$$\mathcal{H}_1 = \sum_{kq} \varPhi_{kq}^\dagger \mathcal{T}_{kq}^f \varPhi_{kq} \,, \tag{18}$$

$$\mathcal{T}_{kq}^f = \sum_{\varDelta s} \left[\mathrm{e}^{iks + iq\varDelta} \left(f_k^\dagger \mathcal{T}_{\varDelta s} f_k \right) + \mathrm{e}^{-iks - iq\varDelta} \left(f_k^\dagger \mathcal{T}_{\varDelta s}^\dagger f_k \right) \right] .$$

Independent of the NT radius there are two bands (A and B say) which intersect the Fermi surface, differing in symmetry properties of the corresponding eigenstates. The minima of the other bands start several tenths of eV away from the FS. We neglect the remaining bands in considering low energy transport properties of these systems. In doing so we assume that neither intertube hopping nor the change δ_H (defined by Eq. (17)) due to crystal lattice potential is strong enough to make admixture of the other bands significant in vicinity of the FS. The same restriction holds for the potential of impurities.

All information about the changes introduced in the electronic structure by the intertube interactions is contained in the matrices' elements $(\mathcal{T}_{kq})_{\mu\nu}$ and $(\delta^f_H)_{\mu\nu} = (f^\dagger_k \delta_H f_k)_{\mu\nu}$ for $\mu,\nu = A, B$. To describe the details of the changes of the FS we have to know the explicit dependence of the matrix upon the wave vectors k, q. Using the results for the unitary transformation f_k derived in Ref. [16] we find

$$\left(f^\dagger_k \mathcal{T}(\varDelta s) f_k\right)_{AA} = \frac{1}{4N_a} \sum_{\mu\nu=1\ldots 2N_a} \Big[\left(V^a(\varDelta s)_{\mu\nu} + V^b(\varDelta s)_{\mu\nu}\right)(-1)^{\nu-\mu}$$

$$+V^{ab}(\varDelta s)_{\mu\nu}(-1)^{\mu-\nu}\mathrm{e}^{ik/2} + V^{ba}(\varDelta s)_{\mu\nu}(-1)^{\mu-\nu}\mathrm{e}^{-ik/2}\Big], \tag{19}$$

$$\left(f^\dagger_k \mathcal{T}(\varDelta s) f_k\right)_{BB} = \frac{1}{4N_a} \sum_{\mu\nu=1\ldots 2N_a} \Big[\left(V^a(\varDelta s)_{\mu\nu} + V^b(\varDelta s)_{\mu\nu}\right)$$

$$- V^{ab}(\varDelta s)_{\mu\nu}\mathrm{e}^{-ik/2} - V^{ba}(\varDelta s)_{\mu\nu}\mathrm{e}^{ik/2}\Big], \tag{20}$$

$$\left(f^\dagger_k \mathcal{T}(\varDelta s) f_k\right)_{AB} = \frac{1}{4N_a} \sum_{\mu\nu=1\ldots 2N_a} \Big[\left(V^a(\varDelta s)_{\mu\nu} - V^b(\varDelta s)_{\mu\nu}\right)(-1)^{\mu}$$

$$+ V^{ab}(\varDelta s)_{\mu\nu}(-1)^{\mu}\mathrm{e}^{-ik/2} - V^{ba}(\varDelta s)_{\mu\nu}(-1)^{\mu}\mathrm{e}^{ik/2}\Big]. \tag{21}$$

We estimated the couplings from Eqs. (19)–(21), by considering (10,10) NTs placed $\Delta R = 0.28$ nm apart (wall–wall distance). In units of intratube NN carbon distance ($= 0.14$ nm), $\Delta R = 2$.

We assumed the hopping between a pair of carbon atoms from different tubes in a form

$$t_{\Delta x,\Delta y,\Delta z} = t_0 \mathrm{e}^{1/r_0} \mathrm{e}^{-\sin(\phi)\Delta R/r_0} \mathrm{e}^{-\sqrt{(\Delta x)^2+(\Delta y)^2}/r_0} \mathrm{e}^{-\Delta z/r_0} \tag{22}$$

with $t_0 = 2t$. Here $\Delta x, \Delta y, \Delta z$ are differences of the two atom coordinates. In Eq. (22) ϕ denotes the angle between a projections to xy plane of a vector joining the pair of carbon atoms and a vector connecting the NTs' axes. Above phenomenological form of the hopping is motivated by the axial NTs' arrangement and takes into account hopping dependence of the angle between the carbon p orbitals. The hopping decay length $r_0 = 0.45$ and $t_0 = 2t$ were chosen to reproduce typical values of the interplane hopping parameters in graphite.

Using the above parameter values we calculated the band shifts due to the intertube hopping interactions for several NT arrangements. The results did depend on the angle between the vertical symmetry plane of the NTs and the triangular lattice unit vector. This was due to the fact that only few of the carbons from different NTs contribute significantly to the band shift ($(\mathcal{T}_{kq})_{AA}$, $(\mathcal{T}_{kq})_{BB}$,) and band coupling ($(\mathcal{T}_{kq})_{AB}$) parameters, and a slight change of the angle modified the hopping substantially. In our numerical calculation we set the angle ϕ to the value which maximized the pseudogap.

For the considered values of r_0 we found that the k-dependence of the band shift and band coupling parameters can be neglected while their q-dependence has to be taken into account. The general form of the parameters can be, to a good approximation, written as

$$(\mathcal{T}_{kq})_{\mu\nu} = p^{(1)}_{\mu\nu}\cos(q_x) + p^{(2)}_{\mu\nu}\cos\left(\frac{q_x}{2} + q_y\right) + p^{(3)}_{\mu\nu}\cos\left(\frac{q_x}{2} - q_y\right) . \qquad (23)$$

The contribution from the on-site potential, δ_H, can be considered in similar way as the diagonal terms of $\mathcal{T}$ for $s = 0$ if we drop the $\mathrm{e}^{iq\Delta}$ factor. In result they do not depend on the wave vectors k, q. The BB contribution, Q_{BB}, is equal this time to AA one and, for positively definite $\delta_{a,b}$, significantly greater than AB contribution, Q_{AB}. This is because of the alternating factors which appear in a formula for Q_{AB} but not in Q_{AA} nor in Q_{BB}. The only effect of Q_{AA} and Q_{BB} on the band structure is a uniform shift of the bands. This can be accounted for by renormalizing a chemical potential. We therefore drop Q_{AA} and Q_{BB} from the subsequent analysis.

Finite AB coupling could have important qualitative effect on the band structure as it removes degeneracy of the A and B band at the FS and opens a gap in the spectrum [24]. Q_{AB} contribution is given by

$$\begin{aligned} Q_{AB} = \sum_{n=1}^{2N_a} \Bigg\{ & U\left[x + \frac{(6n-5)\pi + (-1)^n\pi}{6N_a}\right] \\ & -U\left[x + \frac{(6n-5)\pi - (-1)^n\pi}{6N_a}\right]\Bigg\} (-1)^n . \end{aligned} \qquad (24)$$

In above $U(\phi)$ is a potential function and ϕ is an angle which defines position of the consecutive carbon atoms in the unit cell. $U(\phi)$ is periodic in the argument ϕ with a period 2π and not $2\pi/6$ as could be expected for a triangular lattice. This is because the selfconsistent field created by neighboring NTs has not symmetry of the triangular lattice for general NTs' arrangement. $U(\phi)$ can be defined by its coefficients in Fourier expansion. One can easily see that non vanishing of the l.h.s. of Eq. (24) for (N_a, N_a) NT requires finite value of the Fourier component with $\phi = 4N_a m$ for some integer m. One expects that the component accounting for the symmetry of the triangular lattice ($\phi = 12, 24, 36$) are dominating here. In consequence a rope composed of NTs with $N_a = 3, 6, 9\ldots$ may be quantitatively different from the other ones exhibiting more pronounced gap at the FS. The possible value of this additional contribution is (as inferred from the energy difference of the inequivalent sites in graphite) of order of 0.02 eV. Except the (3,3),(6,6),(9,9)... NTs, it can be probably neglected as compared to intertube hopping contributions.

The solution for the band spectrum resulting from the considered band coupling terms takes a form

$$\begin{aligned} E^{\pm}_{kq} &= \frac{1}{2}\left[(\mathcal{T}_{kq})_{AA} + (\mathcal{T}_{kq})_{BB}\right] \\ &\pm \frac{1}{2}\sqrt{\left[(\mathcal{T}_{kq})_{BB} - (\mathcal{T}_{kq})_{AA} + 2\epsilon_k\right]^2 + 4\,(\mathcal{T}_{kq})_{AB}\,(\mathcal{T}_{kq})_{BA}}\,, \qquad (25) \end{aligned}$$

where $\epsilon_k = t(1 - 2\cos(k/2))$ is the spectrum of AA band of an isolated NT. We have used the above formula to calculate the density of states in the two band system, using the tetrahedron method [23]. The results are presented in Fig. 6.

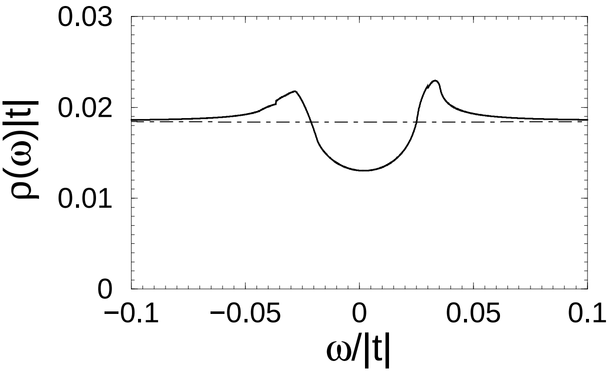

Fig. 6. Density of states for the system of the two bands, described by Eq. (25) in the rope of (10,10) nanotubes for $r_0 = 0.4$. The substantial overlapping of the bands near the FS leads to a finite DOS at $\omega = 0$. The Fermi level for the undoped rope is here $\mu = 0.00154$.

One sees a noticeable reduction in the density of states near the center of the band system. A common feature of the present calculation and of the cited works [24, 26] is existence of the direct gap for (almost) all q vectors near $k = 2\pi/3$. While the order of magnitude of the emerging gap is in a reasonable agreement with the first principles band structure calculation of Delaney and coworkers [24] a reduction of DOS is however less significant than in the cited work. This is due to the fact that the individual subbands overlap substantially in the present calculation. The results for the band structure near FS are also somewhat different from the ones obtained within the full model including all 40 bands, where the values of the band gap are quite close to the two band case. Most important consequence of including the other bands is an effective modification of the band shift term for the symmetric (B) band (the dominating band shift parameter). One may hope to improve the agreement between the present calculation and the first principles ones [24, 26] by choosing the parameters $p_{\mu\nu}$ in Eq. (23) as phenomenological ones, while keeping the form of the band shift and band coupling terms as given by Eq. (23) (we stress that the only adjustable parameter in the present calculation are the intertube hopping t_0, the distance ΔR and the hopping decay length r_0).

In conclusion we note that the intertube interactions remove the degeneracy at the FS, create the pseudogap and at the same time introduce substantial asymmetry near the FS. As will be shown below, this asymmetry may influence substantially the thermopower if the Fermi energy stays within the range of $0.03\,t \sim 0.1$ eV of the band center.

3.2. Conductivity and TEP of ropes of NTs

Intertube interaction considerably complicate calculation of the transport properties of the rope. In the case of strong defects we have to include the intraband as well as the interband scattering for many bands far from the Fermi surface, and the two-band model is certainly inadequate in this case. The use of the Boltzmann transport theory with the energy dependent collision scattering time is not justified which make difficult all the numerical evaluation of TEP. Here we restrict ourselves to a calculation of the transport properties assuming that the relatively numerous weak defects dominate the scattering. We concentrate on the effects of the modification of the band structure due to the intertube interactions. The collision relaxation time may be estimated in this case with a help of the Born approximation as in Eq. (14), with the only difference that the density of states is now modified by the intertube interactions.

In order to compute the conductivity using the Boltzmann transport theory it is convenient to introduce a squared velocity density function defined by

$$\rho_{v^2,\alpha}(\omega) = \frac{1}{N_{\|}N_{\perp}} \sum_{kq} \delta\left(\omega - E^{\alpha}_{kq}\right) v^2_{kq,z} \, . \tag{26}$$

Using $\rho_{v^2\alpha}$ the conductivity at $T = 0$ may be calculated as

$$\sigma(\mu) = e^2 \sum_{\alpha=A,B} \rho_{v^2,\alpha}(\mu)\tau(\mu)\,. \tag{27}$$

The squared velocity density computed with a help of the tetrahedron method, is presented as a function of the Fermi level in the Fig. 7 near $\mu = 0$.

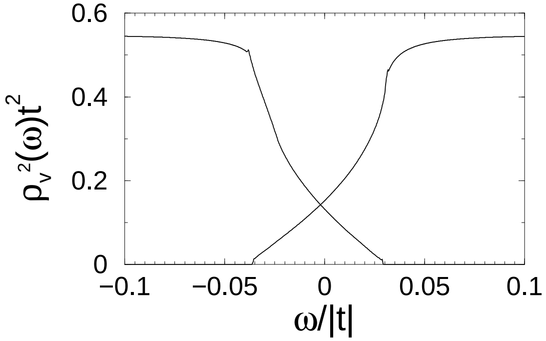

Fig. 7. Squared velocity density function contributions from the two conducting bands (for the direction of nanotube axis).

The two branches of this function overlap at $\mu = 0$, but their sum exhibits a significant minimum at $\mu = 0$. The decrease of the total velocity density is only partially compensated by the increase of the relaxation time resulting from the decreased density of states near the pseudogap minimum. In result, the conductivity at $\mu = 0$ is reduced by about 25% with respect to the original value for the individual NTs (see Fig. 8).

The changes of $\sigma(\mu)$ take place in a relatively small interval of μ values, what leads to considerable values of logarithmic derivative of σ and potentially large TEP at room temperatures (see Fig. 9). From the shape of the pseudogap itself (Fig. 6) one would expect a transition from the strongly hole like behavior of TEP (for $\mu < 0$), to the electron like one, with increase of the Fermi level. The situation is however more complex, which is due to modification introduced by the energy dependence of the relaxation time. In result, the thermopower may change the sign several times within the pseudogap region. One should not take the values shown in Fig. 9 too literally, however. The subtle details of the relaxation time in real systems may depend on a form and a strength of the defect potential or presence of other mechanisms of electron scattering. Besides, disorder in relative arrangement of NTs forming ropes may obliterate rather sharp pseudogap features [25] or lead to cancellation of the contributions from the hole-like and electron-like regions.

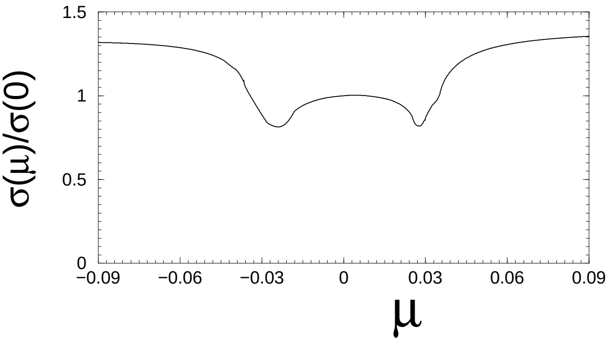

Fig. 8. Conductivity at $T = 0$ K in the vicinity of the pseudogap as a function of the Fermi level, for relaxation time $\tau(\mu)$ computed in the Born approximation, assuming weak defects.

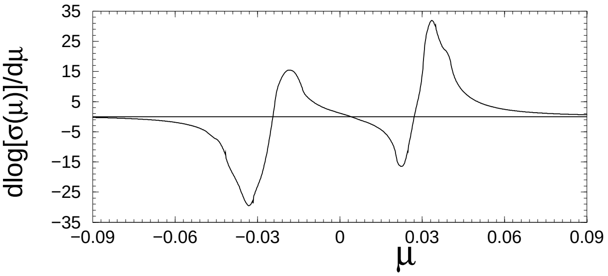

Fig. 9. As in Fig. 8, but the derivative of logarithm of the conductivity at $T = 0$ K.

Quite generally one may expect large absolute values of TEP and a change of sign of TEP (for small enough T) in a relatively small range of doping, $\Delta x \sim 2 \times 10^{-3}$. Beyond the region of the pseudogap (*i.e.* for $|\mu| > 0.2$ eV) the logarithmic derivative of the conductivity quickly goes to the value obtained for the individual NT and the intertube interactions will not influence significantly the TEP.

4. Conclusions

In this paper we discussed influence of electron and hole doping on transport properties of the nanotube ropes within the framework of the tight binding model. We assumed that the defects dominate the charge carrier scattering, and the only effect of introducing the electron or hole donors into the system is the shift of the Fermi level.

The neglect of the usual electron–phonon scattering contribution may be justified by the weakness of electron–phonon coupling in the nanotubes, leading to estimated mean-free path of 14 μm at room temperature (this is at least order of magnitude more than the average NT length) [27]. The consideration of the doping within a rigid band approximation is by no means obvious and should be critically evaluated with a help of *ab initio* computations including presence of doping ions. On the basis of our results one has to conclude that the increase of conductance of rope due to doping cannot be understood as a result of the simple increase of the number of the conducting bands at the Fermi level, assuming that weak defects determine the conductance. As we showed (see Sec.2.2 and Fig. 4), the conductance of the single NT *decreases* in this case, due to the decrease of the relaxation time. A trivial possibility is that the experimentally found increase of σ is a consequence of increase of number of conducting NTs in the sample, due to shift of μ to the conducting bands of the originally semiconducting NTs. An additional mechanism for the increase of σ may be provided by the better screening of the charged defects, due to an increased number of the charge carriers. The importance of this mechanism may be confirmed by the absence of conductance fluctuations in the doped NT rope, as well as the vanishing of the low temperature resistivity upturn in doped mats [11]. The quantitative explanation of the doping dependence of σ will therefore have to take the doping dependence of the screening into account.

The complexity of the experimentally studied systems makes difficult a quantitative comparison of the TEP with results of our computations. In the experimentally studied systems, one may expect a noticeable hole-like contribution to the TEP in mats, coming from the intrinsically semiconducting small-gap NTs, if the Fermi level is lowered by the oxygen adsorbed at the NT's surface. In the similar way, the electron-like TEP obtained in the degassed ropes [13], may be understood if we take into account a possible existence of electron donors (*e.g.* transition metal atoms), left uncompensated in the sample after removing the oxygen.

One would need a more precise control of the position of the Fermi level than currently available in experiments, to verify a possibility that the large value of TEP is a consequence of the intertube interactions. In particular, if we were to see the transition from the hole-like to electron-like TEP within the pseudogap, we would need to control the oxygen concentration to at least 0.001 accuracy (measured as a ratio of oxygen to carbon atoms). On the other hand, the negatively charged oxygen molecules may lead to formation of the quasibound (or quasilocalized) states in the central two-band region of the NTs. This is suggested by *ab initio* computations made for nitrogen substitutional impurity [28], which showed formation of a very clear quasibound state (from its position it can be described by a local defect with

$E_{\rm d}/|t| \sim -2$ within our model). As we showed above, the existence of the quasibound states leads to the minimum of the conductance within the two-band region and may explain transition from the hole-like to electron-like TEP with the Fermi level crossing the position of the quasibound state.

The authors are grateful to P. Eklund, L. Grigorian and G.D. Mahan for numerous helpful discussions. Research support is acknowledged from the University of Tennessee, from Oak Ridge National Laboratory managed by Lockheed Martin Energy Research Corp. for the U.S. Department of Energy under contract DE-AC05-96OR22464, and from a Research Grant No. N00014-97-1-0565 from the Applied Research Projects Agency managed by the Office of Naval Research. This work was also supported in part by the Polish State Committee for Scientific Research (KBN), projects numbers 2 P03B 037 17 and 2 P03B 087 19.

REFERENCES

[1] For a review of experimental and theoretical works on carbon nanotubes, see: R. Saito, G. Dresselhaus, M.S. Dresselhaus, *Physical Properties of Carbon Nanotubes*, Imperial College Press, London 1998.

[2] J. Hone *et al.*, *Phys. Rev. Lett.*, **80**, 1042 (1998).

[3] L. Grigorian *et al.*, *Phys. Rev. Lett.* **80**, 5560 (1998).

[4] J. Hone *et al.*, *Appl. Phys. Lett.* **77**, 666 (2000).

[5] J.W. Mintmire, B.I. Dunlap, C.T. White, *Phys. Rev. Lett.* **68**, 631 (1992).

[6] N. Hamada *et al.*, *Phys. Rev. Lett.* **68**, 1579 (1992).

[7] Z. Wang *et al. Phys. Rev.* **B51**, 13833 (1995).

[8] L. Langer *et al.*, *Phys. Rev. Lett.* **76**, 479 (1996).

[9] A.B. Kaiser, *Phys. Rev.* **B40**, 2806 (1989).

[10] L. Grigorian *et al.*, *Phys. Rev.* **B58**, R4195 (2000).

[11] R.S. Lee *et al.*, *Phys. Rev.* **B61**, 4526 (2000).

[12] P.G. Collins *et al.*, *Science* **287**, 1801 (2000).

[13] G.U. Sumanasekera *et al.*, *Phys. Rev. Lett.* **85**, 1096 (2000).

[14] Ch. Schoenenberger, private communication.

[15] Throughout the paper we use the armchair NT unit cell length, $a = \sqrt{3}d_{\rm C-C} = 0.24$ nm, as our unit length.

[16] T. Kostyrko, M. Bartkowiak, G.D. Mahan, *Phys. Rev.* **B59**, 3241 (1999).

[17] S. Datta, *Electronic Transport in Mesoscopic Systems*, University Press, Cambridge 1995.

[18] T. Kostyrko, M. Bartkowiak, G.D. Mahan, *Phys. Rev.* **B60**, 10735 (1999).

[19] H.J. Choi, J. Ihm, *Solid State Commun.* **111**, 385 (1999).

[20] C.T. White, T.N. Todorov, *Nature* **393**, 240 (1998).

[21] V.H. Crespi, M.L. Cohen, A. Rubio, *Phys. Rev. Lett.* **79**, 2093 (1997).

[22] The summary of the results contained in this section was presented by T. Kostyrko, M. Bartkowiak, G.D. Mahan at the APS March Meeting 99' in Atlanta, Georgia, poster PP01.49.

[23] P.E. Blöchl, O. Jepsen, O.K. Andersen, *Phys. Rev.* **B49**, 16223 (1994).

[24] P. Delaney *et al.*, *Nature* **391**, 466 (1998).

[25] A.A. Maarouf, C.L. Kane, E.J. Mele, *Phys. Rev.* **B61**, 11156 (2000).

[26] J.-C. Charlier, X. Gonze, J.-P. Michenaud, *Europhys. Lett.* **29**, 43 (1995).

[27] T. Hertel, G. Moos, *Phys. Rev. Lett.* **84**, 5002 (2000).

[28] H.J. Choi *et al.*, *Phys. Rev. Lett.* **84**, 2917 (2000).